AIP Journal of Applied Physics

Ferroelectric domain structure of anisotropically strained NaNbO3 epitaxial thin films

J. Schwarzkopf, D. Braun, M. Schmidbauer, A. Duk, and R. Wördenweber

Citation: Journal of Applied Physics **115**, 204105 (2014); doi: 10.1063/1.4876906
View online: http://dx.doi.org/10.1063/1.4876906
View Table of Contents: http://scitation.aip.org/content/aip/journal/jap/115/20?ver=pdfcov
Published by the AIP Publishing

Articles you may be interested in

Anisotropic ferroelectric properties of anisotropically strained epitaxial NaNbO3 films
J. Appl. Phys. **115**, 224103 (2014); 10.1063/1.4882296

Anisotropic one-dimensional domain pattern in NaNbO3 epitaxial thin films grown on (110) TbScO3
Appl. Phys. Lett. **102**, 091903 (2013); 10.1063/1.4794405

Laser beam scanning microscope and piezoresponse force microscope studies on domain structured in 001-, 110-, and 111-oriented NaNbO3 films
J. Appl. Phys. **112**, 052007 (2012); 10.1063/1.4746079

Complex domain structure in relaxed PbTiO3 thick films grown on (100)cSrRuO3//(100)SrTiO3 substrates
J. Appl. Phys. **112**, 052001 (2012); 10.1063/1.4746078

Local retention behaviors of epitaxial and polycrystalline Pb Mg 1 3 Nb 2 3 O 3 – PbTi O 3 thin films by scanning force microscopy
Appl. Phys. Lett. **91**, 072906 (2007); 10.1063/1.2769945

Re-register for Table of Content Alerts

Create a profile.

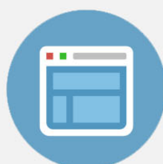

Sign up today!

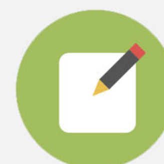

[This article is copyrighted as indicated in the article. Reuse of AIP content is subject to the terms at: http://scitation.aip.org/termsconditions. Downloaded to] IP: 134.94.122.17 On: Wed, 18 Jun 2014 12:54:53

JOURNAL OF APPLIED PHYSICS 115, 204105 (2014)

Ferroelectric domain structure of anisotropically strained $NaNbO_3$ epitaxial thin films

J. Schwarzkopf,[1,a)] D. Braun,[1] M. Schmidbauer,[1] A. Duk,[1] and R. Wördenweber[2]
[1]*Leibniz-Institute for Crystal Growth, Max-Born-Str. 2, 12489 Berlin, Germany*
[2]*Forschungszentrum Jülich, Peter Grünberg Institute, Jülich, Germany*

(Received 24 March 2014; accepted 4 May 2014; published online 28 May 2014)

$NaNbO_3$ thin films have been grown under anisotropic biaxial strain on several oxide substrates by liquid-delivery spin metalorganic chemical vapor deposition. Compressive lattice strain of different magnitude, induced by the deposition of $NaNbO_3$ films with varying film thickness on $NdGaO_3$ single crystalline substrates, leads to modifications of film orientation and phase symmetry, which are similar to the phase transitions in Pb-containing oxides near the morphotropic phase boundary. Piezoresponse force microscopy measurements exhibit large out-of-plane polarization components, but no distinctive domain structure, while C-V measurements indicate relaxor properties in these films. When tensile strain is provoked by the epitaxial growth on $DyScO_3$, $TbScO_3$, and $GdScO_3$ single crystalline substrates, $NaNbO_3$ films behave rather like a normal ferroelectric. The application of these rare-earth scandate substrates yields well-ordered ferroelectric stripe domains of the type a_1/a_2 with coherent domain walls aligned along the [001] substrate direction as long as the films are fully strained. With increasing plastic lattice relaxation, initially, a 2D domain pattern with still exclusively in-plane electric polarization, and finally, domains with in-plane and out-of-plane polar components evolve. © *2014 AIP Publishing LLC*. [http://dx.doi.org/10.1063/1.4876906]

INTRODUCTION

Domain properties in ferroelectric thin films are currently in the focus of fundamental research. Their size and symmetry as well as the nature of the domain walls have large impact on the ferro- and piezoelectric properties of thin films. Consequently, understanding and controlling of domains are essential for further application in nanometer sized electronic devices. Domain formation critically depends on the incorporated lattice strain induced by the substrate (lattice parameter and symmetry mismatch between film and substrate material), the composition, and stoichiometry of the film as well as the nature and density of defects.[1–6]

Incorporation of lattice strain in thin films by the heteroepitaxial growth on lattice mismatched substrates can have a beneficial effect on film properties. For example, it provides the stabilization of ferroelectric phases which are not found in the bulk parent compounds,[1,7] or leads to a significant increase of the remnant polarization and a shift of the Curie temperature.[8,9] Theoretical descriptions of strain-phase diagrams with regard to biaxial isotropic lattice strain have been provided by the fundamental work of Pertsev *et al.*[10] within the Landau-Ginzburg-Devonshire theory and by *ab-initio* calculations performed by Diéguez *et al.*[11] for several perovskite based materials. For isotropic in-plane lattice strain in $NaNbO_3$ films, transitions from a tetragonal phase (T) with only an out-of-plane polarization component ($P_1 = P_2 = 0$ and $P_3 \neq 0$) to a monoclinic or rhombohedral phase (R) with both an in-plane and out-of-plane component of the polarization ($P_1 = P_2 \neq 0$ and $P_3 \neq 0$) and finally to an orthorhombic phase (*aa*) with exclusive in-plane polarization ($P_1 = P_2 \neq 0$ and $P_3 = 0$) with increasing in-plane lattice parameter have been predicted.

Generally, due to the orthorhombic symmetry of most oxide substrates and many perovskite films, substrate induced biaxial lattice strain in thin films is non-uniform, which, however, has rarely been investigated yet. This in-plane anisotropy in epitaxial mismatch strain can reduce the group symmetry of film structure, which is different to the case of biaxial isotropic strain state and may result in larger stability regions of rotational single-domain phases or multi-domain states.[12] Single-domain phase diagrams have been theoretically predicted from non-linear thermodynamic simulations,[13–16] where the formation of misfit dislocations or of ferroelastic domains to reduce energy has not been considered. Stability maps consisting of single- and multi-domain phase regions have been deduced by phase field simulations[17,18] and a full scale nonlinear thermodynamic model[12,19,20] taking into account of lattice relaxation by misfit dislocations, to the contribution of micro-strain for multi-domain formation and to electrical boundary conditions (depolarization field).

A very low number of reports have described experimental results on the influence of anisotropic in-plane strain on domain formation of ferroelectric thin films.[21–24] Mostly, film-substrate combinations have been considered, theoretically as well as experimentally, where a film material with a cubic or tetragonal structure at room temperature (RT) (like $PbZr_{1-x}Ti_xO_3$ with $x = 0.7 - 1$, $PbTiO_3$ or $Ba_{1-x}Sr_xTiO_3$ with $x = 0 - 1$) is grown on an orthorhombic substrate (like $NdGaO_3$ or the rare-earth scandates). $NaNbO_3$ based materials have attracted much interest from scientific as well as potentially practical point of view due to their promising ferro- and piezoelectric properties,[25] complexity of phase

a)Electronic mail: jutta.schwarzkopf@ikz-berlin.de

 © 2014 AIP Publishing LLC

[This article is copyrighted as indicated in the article. Reuse of AIP content is subject to the terms at: http://scitation.aip.org/termsconditions. Downloaded to] IP: 134.94.122.17 On: Wed, 18 Jun 2014 12:54:53

transitions and interesting electric behavior under the influence of applied electric field or lattice strain.[26–30] However, $NaNbO_3$ undergoes a phase transition from a para- to an antiferroelectric phase at 633 K and crystallizes at RT in the orthorhombic P phase[28] (space group *Pbcm)* in contrast to the above mentioned materials.

In this paper, we report about the first systematic study on the anisotropic strain impact on domain configuration in $NaNbO_3$ thin films grown by liquid-delivery spin metal-organic chemical vapor deposition (MOCVD). The deposition of $NaNbO_3$ in thin film form is rather challenging due to the high volatility of the alkaline component. We will show that on the one hand polarization direction and piezoelectric coefficient are critically influenced by the incorporation of lattice strain and substrate symmetry. On the other hand, domain size and ordering also can be changed from a relaxor ferroelectric state to well-ordered ferroelectric stripe domains by incorporation of anisotropic compressive and tensile lattice strain, respectively, while the deposition conditions are kept constant.

EXPERIMENTAL

Film deposition and characterization

Epitaxial $NaNbO_3$ films were grown by liquid-delivery spin MOCVD on 0.1° off-oriented $NdGaO_3$(110), $DyScO_3$(110), $TbScO_3$(110), and $GdScO_3$(110) single crystalline substrates. Before introducing the perovskite substrates into the reactor chamber, they were annealed in pure oxygen gas flow at 1050 °C for $NdGaO_3$, $GdScO_3$, and $DyScO_3$ and at 1150 °C for $TbScO_3$ in order to generate a regular step-and-terrace surface structure with ~200 nm broad atomically smooth terraces and step heights of one monolayer (~4 Å).[31,32] All $NaNbO_3$ films with thickness ranging from ~10 nm to 140 nm were deposited at a substrate temperature of 700 °C and an O_2 to Ar ratio in the gas phase of 0.63 at a gas pressure of 2.6×10^3 Pa. The Na(thd) ((thd) = 2,2,6,6-tetramethyl-3, 5-heptanedione) and $Nb(EtO)_5$ ($(EtO)_5$ = penta-ethoxide) metal-organic precursors dissolved in dry toluene with a concentration of 0.01 M were evaporated at 230 °C and 190 °C, respectively, and transported by Ar as carrier gas into the reactor chamber via a showerhead. More details of the deposition parameters are described in Ref. 33.

Strain state and film thickness were assessed by high-resolution x-ray diffraction (HRXRD). A precollimating parabolic multilayer mirror was employed in front of a 2-bounce Ge 220 channel-cut monochromator which was utilized to select the Cu Kα_1 line at $\lambda = 1.54056$ Å and to further collimate the incident x-ray beam. Primary slits were used to define the beam size at the sample to 0.3 mm × 5 mm. Reciprocal space maps (RSM) were recorded by using a linear position sensitive detector which simultaneously measured the direction of the diffracted beam with an accuracy of about 0.01°. The RSMs were taken by a single rocking scan of the sample while the detector was kept fixed. For further details of this technique, see Ref. 34. From the RSMs, the out-of-plane and in-plane lattice parameters of the films were determined taking the well known Bragg reflections of the substrate as reference. The position sensitive detector can be also used as a single channel detector, and x-ray rocking curves were measured in symmetrical scattering geometry for complementary information for the out-of plane strain.

In order to obtain more detailed information about the in-plane lattice strains in the $NaNbO_3$ films, grazing incidence x-ray diffraction (GIXRD) were performed by using highly brilliant synchrotron radiation at BW2 beam line at HASYLAB/DESY and at KMC-2 beam line at BESSY. The glancing angle of incidence was chosen close to the critical angle of total external reflection with the aim to adapt the x-ray penetration depth to the film thickness.

The surface morphology of the films was analyzed via atomic force microscopy (AFM, Asylum Research MFP3D standalone). The respective domain structures and local effective piezoelectric out-of-plane responses ($d^{eff}{}_{zz}$) were analyzed by the piezoresponse force microscope (PFM) setup of the AFM utilizing the dual ac resonance tracking (DART) mode.[35] Piezoelectric characterization of the domains was performed by in-plane (lateral PFM or LPFM) as well as out-of-plane (vertical PFM or VPFM) measurements. In-plane measurements were conducted in two in-plane alignments, which differ by an in-plane rotation of the sample by 90° (x-LPFM and y-LPFM).

Transformation from orthorhombic lattice parameters to pseudocubic lattice parameters

Bulk $NaNbO_3$ crystallizes at RT in the P phase with orthorhombic crystal symmetry ($a_o = 5.569$ Å, $b_o = 5.505$ Å, and $c_o = 15.523$ Å,[36] *Pbcm* setting). However, for the description of non-cubic perovskite materials, the lattice parameters are often given in pseudocubic notation. In our earlier publication,[33] we neglected that anisotropic strain is introduced when a film with unequal in-plane lattice parameters is grown on a cubic or even orthorhombic substrate; only the average in-plane strain was considered. Since, however, in-plane anisotropy is crucial for domain formation here we use the relationship between the orthorhombic and pseudocubic systems given in Ref. 37. On the basis of these considerations, we have calculated the pseudocubic lattice parameters of $NaNbO_3$ to $a_c = 3.881$ Å, $b_c = 3.915$ Å, $c_c = 3.915$ Å, and $\alpha_c = 90.67°$. A schematic presentation of the orthorhombic *Pbcm* and the inscribed pseudocubic unit cell is shown in Fig. 1(a). In the following, the suffixes "c" and "o" are used for the pseudocubic and the orthorhombic notation, respectively.

Lattice mismatch and film orientation on the different substrates

Epitaxial growth on lattice mismatched substrates leads to elastic deformations in films. For a thin film with homogenous strain the effect of strain on the free energy density is generally described by using Hooke's law[38]

$$F(\varepsilon) = \frac{1}{2}\sum\nolimits_{klmn} C_{klmn}\varepsilon_{kl}\varepsilon_{mn} \quad \text{with} \quad k, l, m, n = x, y, z, \quad (1)$$

where C_{klmn} and ε_{kl} denote the elastic coefficients of the film and the strain tensor, respectively. For epitaxial, biaxially

[This article is copyrighted as indicated in the article. Reuse of AIP content is subject to the terms at: http://scitation.aip.org/termsconditions. Downloaded to] IP: 134.94.122.17 On: Wed, 18 Jun 2014 12:54:53

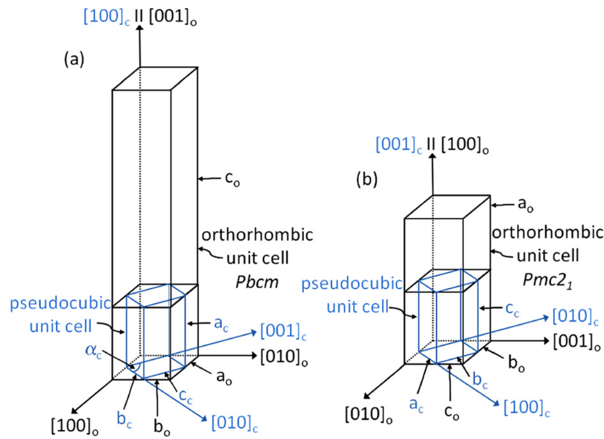

FIG. 1. Schematic presentation of the orthorhombic (black lines) and inscribed pseudocubic unit cells (blue lines) of $NaNbO_3$ for (a) Pbcm symmetry and (b) $Pmc2_1$ symmetry.

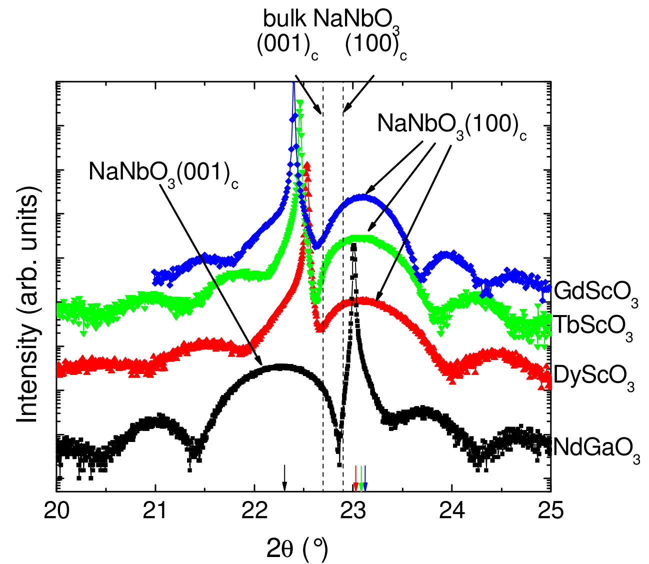

FIG. 2. HRXRD pattern (2θ–ω scans) of 10 nm $NaNbO_3$ films on different substrates in the 2θ range between 20° and 25°. The corresponding substrates are listed on the right side of the diagram. The dotted lines indicate the angular positions of the $(001)_c$ and $(100)_c$ Bragg peaks of bulk $NaNbO_3$ (P phase). The arrows at the bottom of the diagram tag the maximum position of the film Bragg reflections, from which we determined the out-of-plane lattice parameters (see Table II).

strained film growth with traction-free surfaces and without shear strain,[39] the strain tensor is reduced to the two in-plane normal components ε_{xx} and ε_{yy} corresponding to the lattice mismatch between film (bulk lattice parameter: a_f) and substrate material (lattice parameter: a_s) defined by $\varepsilon = (a_f - a_s)/a_f$. Since film and substrates have an orthorhombic symmetry, the normal components ε_{xx} and ε_{yy} are non-equal. We have estimated the free energy density for $NaNbO_3$ film growth on the different substrates taking into consideration that (i) the $NaNbO_3$ thin films can be deposited with $(100)_c$, $(010)_c$, or $(001)_c$ surface orientation and (ii) two variants, which differ by an in-plane rotation of 90°, are possible. Principally, six different variations are possible, however, since b_c is equal to c_c from the elastic point of view, the number of independent configurations is reduced: on the one hand, for a_c oriented films 90° in-plane variants are not distinguishable and on the other hand, b_c oriented and c_c oriented films exhibit the same in-plane parameters. Hence, due to symmetry reasons only three independent orientations of $NaNbO_3$ have to be considered and are given in Table I. Since data for $NaNbO_3$ are not available the elastic coefficients for $KNbO_3$[40] are used for this quantification. From Table I, it can be inferred that $NaNbO_3$ thin films on $NdGaO_3$ substrates will grow with $(001)_c$ surface orientation under compressive strain, while tensile in-plane strain and $(100)_c$ film orientation is favored to be incorporated in films on the rare-earth scandates.

RESULTS AND DISCUSSION

$\theta/2\theta$ HRXRD scans in the 2θ range between 10° and 90° have demonstrated the deposition of single-phase $NaNbO_3$ thin films on all substrates.[33] Higher magnified HRXRD patterns around the $(110)_o$ Bragg reflection of the orthorhombic substrates clearly show that the peak position provoked by $NaNbO_3$ thin films depends on the choice of the substrate (see Fig. 2 for 10 nm thick films). The occurrence of thickness oscillations implies that all films exhibit smooth surfaces and interfaces as well as a well-ordered film structure. Broadening of film contributions is caused by the small film thickness. At a film thickness of ~10 nm all films were grown fully strained on the substrate, indicated by the fact that the in-plane lattice parameters of the films are commensurate to those of the substrate. This is shown in Fig. 3 by RSMs in the

TABLE I. Lattice parameters of the surface unit cell of the different oxide substrates and calculated free energy densities (in GPa) according to Eq. (1) for the three different variants of strained $NaNbO_3$ thin films. In the right column, the in-plane lattice mismatches $\varepsilon_{xx}/\varepsilon_{yy}$ for the film orientation with the lowest free energy density (grey highlighted) are given. The suffixes "c" and "o" label the pseudocubic notation of the $NaNbO_3$ films and the orthorhombic coordinate system of the substrates, respectively.

	Surface unit cell of the substrate (Å)		Free energy density (GPa)			In-plane lattice mismatch
			$(100)_c$ film orient.	$(001)_c$ film orientation		
Substrate	In $[1\text{-}10]_o$ direction	In $[001]_o$ direction	In-plane: $[010]_c\|\|[-110]_o$ and $[001]_c\|\|[001]_o$	In-plane: $[100]_c\|\|[-110]_o$ and $[010]_c\|\|[001]_o$	In-plane: $[010]_c\|\|[-110]_o$ and $[100]_c\|\|[001]_o$	ε_{xx} in $[1\text{-}10]_o$ / ε_{yy} in $[001]_o$
$NdGaO_3(110)$	2 × 3.863	2 × 3.854	7.40×10^{-2}	4.29×10^{-2}	3.58×10^{-2}	1.34 / 0.69
$DyScO_3(110)$	2 × 3.947	2 × 3.952	2.76×10^{-2}	6.10×10^{-2}	6.84×10^{-2}	−0.81 / −0.94
$TbScO_3(110)$	2 × 3.960	2 × 3.959	4.52×10^{-2}	8.70×10^{-2}	9.35×10^{-2}	−1.14 / −1.12
$GdScO_3(110)$	2 × 3.970	2 × 3.966	6.39×10^{-2}	1.13×10^{-1}	1.19×10^{-1}	−1.40 / −1.29

[This article is copyrighted as indicated in the article. Reuse of AIP content is subject to the terms at: http://scitation.aip.org/termsconditions. Downloaded to] IP: 134.94.122.17 On: Wed, 18 Jun 2014 12:54:53

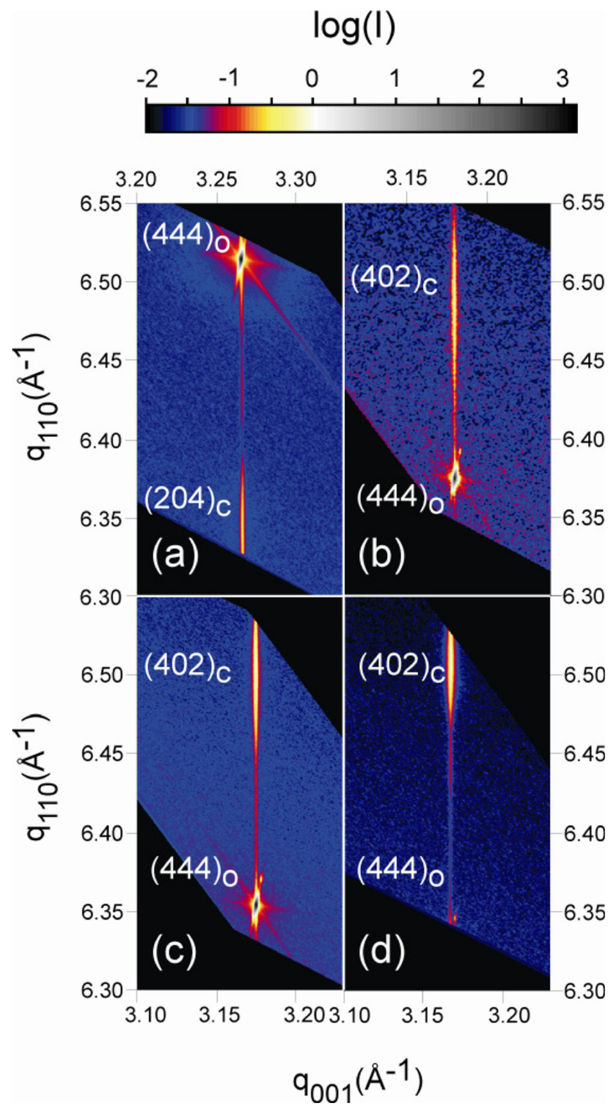

FIG. 3. X-ray reciprocal space maps in the vicinity of the $(444)_o$ Bragg reflection of the substrates for 10 nm thin films grown on a $NdGaO_3$ (a), $DyScO_3$ (b), $TbScO_3$ (c), and $GdScO_3$ (d).

vicinity of the $(444)_o$ reflection peak of the orthorhombic substrates. Identical results were achieved also in $[1–10]_o$ direction in the vicinity of the $(260)_o$ and $(620)_o$ substrate Bragg peaks, which are not shown here. Careful evaluation of the peak position of the film contributions in the 2θ–ω scans in Fig. 2 proves that the 2θ angle of the film peak decreases, and

TABLE II. Pseudocubic out-of-plane lattice parameter $d_\perp$, film orientation and in-plane strain state of 10 nm thick, fully strained $NaNbO_3$ films on the different oxide substrates as well as change of the relative unit cell volume $\Delta V/V = (V_f - V_b)/V_b$, where V_f and V_b are the unit cell volumes of the strained $NaNbO_3$ films and of unstrained $NaNbO_3$, respectively. V_b is calculated from the pseudocubic lattice parameters of bulk $NaNbO_3$ to 59.48 Å.

	$NdGaO_3(110)o$	$DyScO_3(110)o$	$TbScO_3(110)o$	$GdScO_3(110)o$
$d_\perp$	3.984 Å	3.849 Å	3.848 Å	3.846 Å
Film orientation	$(001)_c$	$(100)_c$	$(100)_c$	$(100)_c$
In-plane strain	Compressive	Tensile	Tensile	Tensile
$\Delta V/V$	−0.3%	0.9%	1.4%	1.8%

accordingly, the out-of-plane lattice parameter of the films $d_\perp$ successively increases with decreasing in-plane lattice parameters of the film (see arrows on the 2θ axis in Fig. 2 and Table II, respectively). Furthermore, the lattice mismatch between $NaNbO_3$ and the different used substrates has a decisive influence not only on the strain state, but also on the surface orientation of the films. From the position of the film Bragg peaks relative to the substrate Bragg peaks and the position of unstrained $(001)_c$ and $(100)_c$ oriented $NaNbO_3$, we conclude that films on $NdGaO_3$ are grown with $(001)_c$ surface orientation under compressive strain, while the application of the rare-earth scandates as substrates leads to $(100)_c$ oriented film growth under tensile lattice strain. These results agree well with the findings from elasticity theory given from Table I. Since in-plane lattice parameters of the substrates are not equal, all films are anisotropically strained (see also Table I, ε_{xx} and ε_{yy}).

Figures 4 and 5 show the morphology of $NaNbO_3$ films on the different substrates and the phase images of VPFM and LPFM measurements in the two orthogonal in-plane directions (x-LPFM and y-LPFM) of ∼30 nm thick films on the different substrates. All films exhibit very smooth surfaces with an average roughness ≤0.3 nm. Domain patterns can be observed for all samples, however, depending on the choice of substrate the PFM results differ significantly in signal strength as well as in shape and alignment of the domains. In the following sections the results obtained for the different strain states (i.e., compressive strain for films on $NdGaO_3$ and tensile strain for films on the rare-earth scandates) will be discussed separately. The emphasis of this discussion lies on the domain formation and its relation to the phase symmetry of the epitaxially grown films.

Fully compressively strained films on $NdGaO_3$

For thin films (d ≈ 10 nm), the RSM image reveals that both in-plane components of the scattering vectors of the $NaNbO_3(024)_c$ and $(204)_c$ Bragg reflections are identical to those of the $(444)_o$ and $(260)_o$ reflections of the $NdGaO_3$ substrate (exemplarily shown for $(444)_o$ in Fig. 3(a)). This proves fully coherent film growth of $NaNbO_3$ on the $NdGaO_3$ substrate. Also high-resolution transmission electron microscopy (HRTEM) images, shown in our recent publication,[33] confirm pseudomorphic film growth on $NdGaO_3$. The HRTEM data of the film can be simulated by an orthorhombic *Pmc2₁* structure with the orthorhombic $[100]_o$ axis parallel to the surface normal. We choose here a pseudocubic unit cell of $NaNbO_3$ which is inscribed in the orthorhombic *Pmc2₁* unit cell such that the $[001]_c$ axis coincide with the orthorhombic $[100]_o$ axis and the pseudocubic cell is rotated in-plane by 45°, i.e., $[100]_c \parallel [011]_o$ and $[010]_c \parallel [0\text{-}11]_o$ (see Fig. 1(b)). The *Pmc2₁* is a polar phase, which belongs to the point group *mm2* with polar axis in $\langle 111\rangle_o$ in the orthorhombic system[41] (and accordingly in $\langle 101\rangle_c$ in the pseudocubic unit cell). It has also been observed by Shiratori *et al.*[42] for submicrocrystalline $NaNbO_3$ particles under ambient pressure.

Vertical and lateral PFM amplitude measurements indicate the existence of both a very strong out-of-plane and an in-plane component of the polarization. This agrees well with the fact that the polarization direction of an orthorhombic

[This article is copyrighted as indicated in the article. Reuse of AIP content is subject to the terms at: http://scitation.aip.org/termsconditions. Downloaded to] IP: 134.94.122.17 On: Wed, 18 Jun 2014 12:54:53

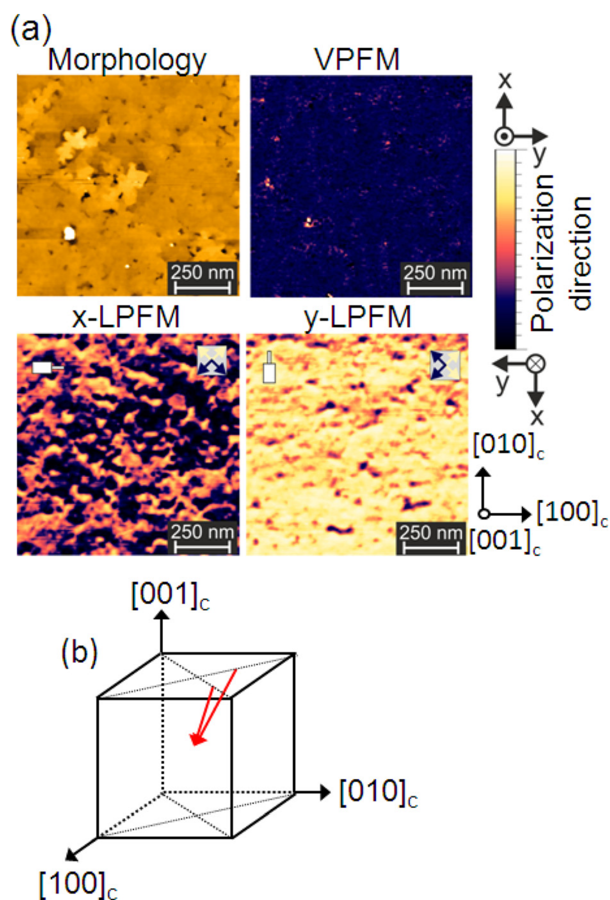

FIG. 4. (a) Morphology, vertical, and lateral PFM phase images of a ∼30 nm thick $NaNbO_3$ film on $NdGaO_3$. x-PFM and y-PFM mark the two orthogonal in-plane scan directions, relative position of the cantilever to the sample is depicted in the left upper part of the PFM images. (b) Schematic presentation of the possible directions of the polarization vector.

mm2 phase is oriented along $\langle 111\rangle_o$ in the orthorhombic unit cell (respective the $\langle 101\rangle_c$ direction in the pseudocubic unit cell) and is schematically presented in Fig. 6(a) by the arrow which ends at point O. Since amplitude and phase images of the LPFM and VPFM measurements exhibit no contrasts and nearly no domain-related features are discernible, we do not show the PFM measurements on 10 nm thin films here. The absence of any contrasts in PFM measurements also has been observed in literature for $Bi_{1/2}Na_{1/2}TiO_3$-$BaTiO_3$ derived ceramics[43] and $PbMg_{1/3}Nb_{2/3}O_3$ thin films[44] and was attributed to relaxor properties of the samples.

It should be noted that the occurrence of an in-plane polar component cannot be explained if the in-plane anisotropy of lattice strain is neglected. For isotropic biaxial strain, Diéguez *et al.*[11] predicted that highly compressively strained films exist in a ferroelectric phase with tetragonal symmetry. However, no lateral PFM response would be expected for such a tetragonal phase (corresponding polarization vector should end at point T in Fig. 6(a)) in contradiction to our PFM results.

Partially relaxed films on $NdGaO_3$

With increasing film thickness ($d \geq 15$ nm), film lattice starts to plastically relax by the formation of defects. This is manifested by a decrease of the out-of-plane lattice parameter with increasing thickness.[33] Up to a thickness of ∼30 nm, the RSMs recorded in the vicinity of the $(260)_o$ and $(444)_o$ Bragg reflections of the $NdGaO_3$ substrate show single $(204)_c$ and $(024)_c$ film reflection peaks only, which are slightly broadened and shifted to higher q_{110} values due to the onset of plastic strain relaxation. This implies that the orthorhombic phase is still retained.

With further increased film thickness, we still observe a single $(024)_c$ film contribution, while the $(204)_c$ $NaNbO_3$ film peak is equally split (shown for a 50 nm thick film in Fig. 7). The splitting of a $(h0l)_c$ reflection peak points to the formation of the monoclinic M_A phase (notation of Vanderbilt and Cohen[45] is used).[46,47] In monoclinic M_A phases, the polarization vector is aligned along $\langle uuv\rangle_c$ with $u < v$ and can freely rotate in a $\{110\}_c$ plane. This is schematically presented in Fig. 6(a) by the arrow ending at point M_A.

Similar to the measurements on fully strained films, the PFM amplitude signal of ∼30 nm thick films on $NdGaO_3$ confirms the presence of a strong vertical and a weaker lateral piezoresponse. The PFM phase images in Fig. 4(a) are typical for $NaNbO_3$ films grown on $NdGaO_3$ substrates with film thicknesses between 10 and ∼140 nm. The vertical phase image is uniformly dark seemingly implying that the polarization vector is exclusively directed into the film plane. The two orthogonal LPFM measurements indicate that the polarization vector is aligned in $[\pm uuv]_c$ with $u < v$ (schematically presented in Fig. 4(b) by the two arrows) which is consistent with the M_A symmetry derived from HRXRD.

The almost exclusive top-down arrangement of the polarization vector would be surprising suggesting the formation of a monodomain. This is, however, energetically unfavorable, when no bottom or top electrode is used. Wördenweber *et al.* have shown that our compressively strained $NaNbO_3$ films on $NdGaO_3$ exhibit relaxor behavior.[48] The assumption of a ferroelectric relaxor would explain the observation of strong vertical PFM amplitude signals together with a uniform phase image without contrast in an unpoled state. In relaxors, weakly interacting polar nanometer-size regions are formed, leading to low polarization contrast, uniformly distributed directions of the dipole moments and diffuse domain walls.[44] Similar results have been described for compressively strained $BiFeO_3$ thin films on $LaAlO_3$ substrates[47] and $Bi_{1/2}Na_{1/2}TiO_3$-$BaTiO_3$ ceramics,[43] which exhibit likewise relaxor properties. Ongoing advanced experiments regarding the domain switching after DC poling and relaxation as well as temperature dependent PFM have also suggested relaxor behavior. These results go beyond the scope of this paper and will be described in a future publication.

Fully tensily strained films on $ReScO_3$ with Re = Dy, Tb, Gd

HRXRD reciprocal space maps of $NaNbO_3$ films on $TbScO_3$ substrates verify pseudomorph film growth up to a film thickness of about 20 nm.[24] All films on $TbScO_3$ exhibit slightly reduced out-of-plane lattice parameters (between 3.849 Å and 3.864 Å for films with a thickness between 10 nm and 66 nm) compared to relaxed $(100)_c$ oriented $NaNbO_3$ which indicates the incorporation of tensile in-plane lattice strain. From GIXRD investigations, we

[This article is copyrighted as indicated in the article. Reuse of AIP content is subject to the terms at: http://scitation.aip.org/termsconditions. Downloaded to] IP: 134.94.122.17 On: Wed, 18 Jun 2014 12:54:53

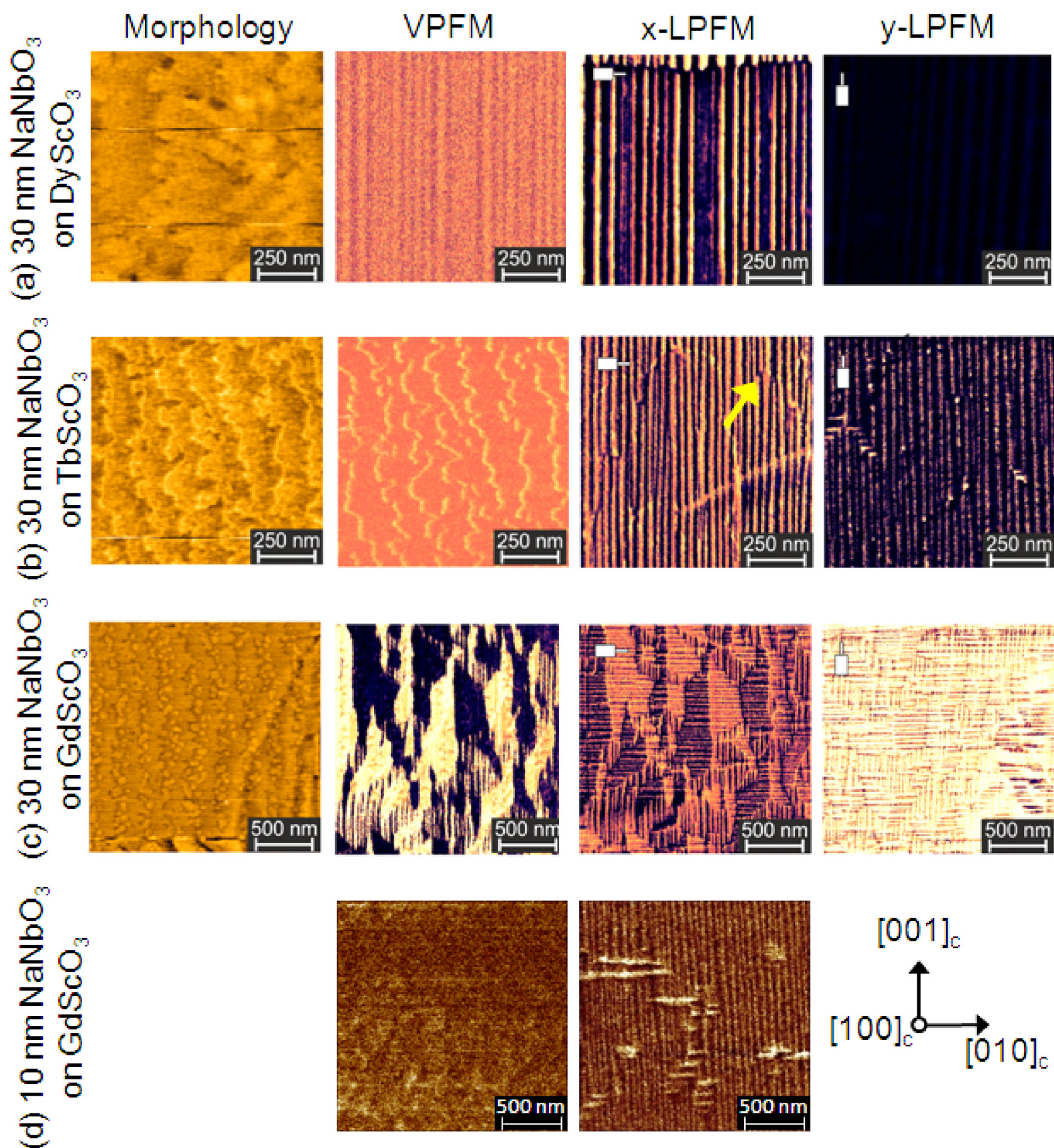

FIG. 5. Morphology, vertical, and lateral PFM phase images of ∼30 nm thick $NaNbO_3$ films on (a) $DyScO_3$, (b) $TbScO_3$, and (c) $GdScO_3$. x- and y-LPFM differ by a 90° in-plane rotation of the sample, relative position of the cantilever to the sample is depicted in the left upper part of the PFM images. (d) VPFM and LPFM images of a 10 nm thick $NaNbO_3$ film on $GdScO_3$.

concluded that these films consist of two types of monoclinic domains which differ by an in-plane monoclinic distortion $\pm\,\beta^*$ of the unit cell with respect to the $[1\text{-}10]_o$ (or $[100]_c$) direction[24] (see Fig. 8(a)). The monoclinic distortion angle β^* increases with increasing film thickness and approaches the maximum value of $\beta^*_{max} \approx 0.67°$ for a film thickness $d \approx 20$ nm. For even thicker films, β^* remains at β^*_{max} which is in agreement with the monoclinic bulk angle of 0.67° reported for the P phase of $NaNbO_3$ at RT.[49] On the basis of GIXRD, we also established that the crystal lattice at domain walls between adjacent domains remains coherent. Similar results are obtained for fully strained films on $DyScO_3$ substrates,[50] where commensurate film growth is preserved for films up to a thickness of ∼30 nm. This is attributed to the lower lattice mismatch (see Table I). Since the lattice mismatch for $NaNbO_3$ thin films on $GdScO_3$ substrate is still higher, we have observed the onset of plastic relaxation due to formation of defects (also displayed by the slight broadening of the film contribution in Fig. 3(d)) even for the thinnest film (∼10 nm film thickness).

PFM phase measurements on $NaNbO_3$ thin films on $TbScO_3$ and $DyScO_3$ exhibit quite similar features (Figs. 5(a) and 5(b), respectively). In the x-LPFM images, a pronounced arrangement of periodic stripes in $[001]_o$ (or $[001]_c$) direction with alternating dark and bright contrast can be observed, whereas the LPFM phase images in the orthogonal

[This article is copyrighted as indicated in the article. Reuse of AIP content is subject to the terms at: http://scitation.aip.org/termsconditions. Downloaded to] IP: 134.94.122.17 On: Wed, 18 Jun 2014 12:54:53

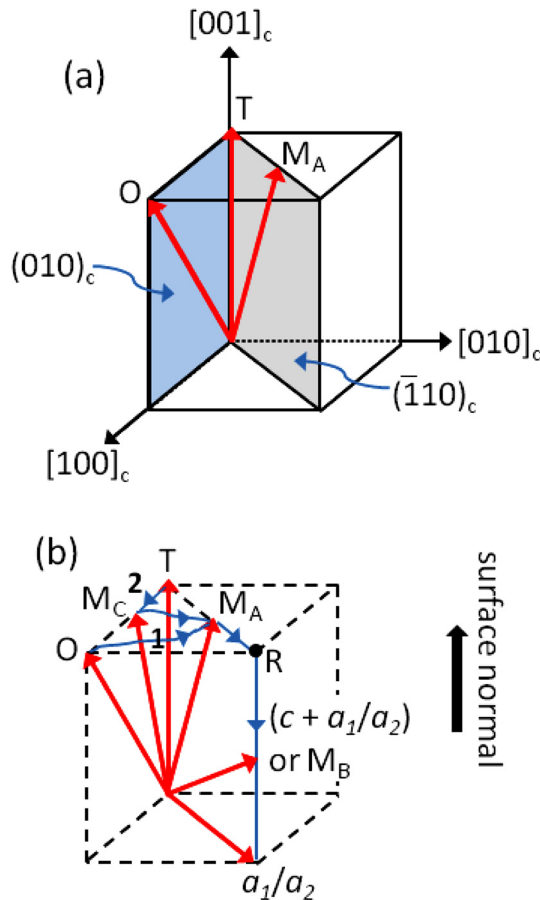

FIG. 6. (a) Schematic presentation of the orientation of the polarization vector in the orthorhombic *mm2* (O), the tetragonal (T) and the monoclinic M_A phase. (b) Trajectory of the polarization directions with increasing in-plane lattice parameter. "1" describes the phase transition pathway from the orthorhombic O to the monoclinic M_A phase, while path "2" has been observed for $BiFeO_3$ films on $LaAlO_3$ (46).

direction (y-LPFM) show a lower contrast. The VPFM phase images exhibit only marginal variations. Together with relatively low piezoresponse amplitudes in VPFM, we suppose the absence of any vertical component of the polarization vector. The observed slight striation is attributed to a cross-talk between vertical and lateral channel detection caused by the strong lateral piezoresponse signal. From these results, we deduce that the polarization vector is aligned along the $\langle 011\rangle_c$ directions of the pseudocubic unit cell of $NaNbO_3$ marked by red arrows in Fig. 8(a) (notice, that films on the $ReScO_3$ substrates are $(100)_c$ oriented, i.e., the pseudocubic $[010]_c$ and $[001]_c$ directions are in the film plane, see Fig. 1(a)). However, since the lattice parameters of the film's unit cell b_c and c_c are unequal due to the anisotropy of the substrate unit cell, the direction of the polarization is assumed to slightly deviate from the $\langle 011\rangle_c$. The polarization vectors between neighboring domains enclose an angle of almost 90° from which we infer an a_1/a_2 multi-domain configuration[24,51,52] (see schematic drawings in Fig. 8(a) and the lower arrows in Fig. 8(b), from bird view and side view, respectively).

Even though all films are deposited under the same deposition conditions, the films grown on the rare-earth scandates are assumed to exhibit a slight deviation from the nominal stoichiometry. This is deduced for fully strained films from the change of the relative unit cell volume $\Delta V/V = (V_f - V_b)/V_b$, where V_f and V_b are the unit cell volumes of the strained $NaNbO_3$ film and of unstrained $NaNbO_3$, respectively. From Table II, it is striking, that the film unit cell volumes are decreased (increased) for

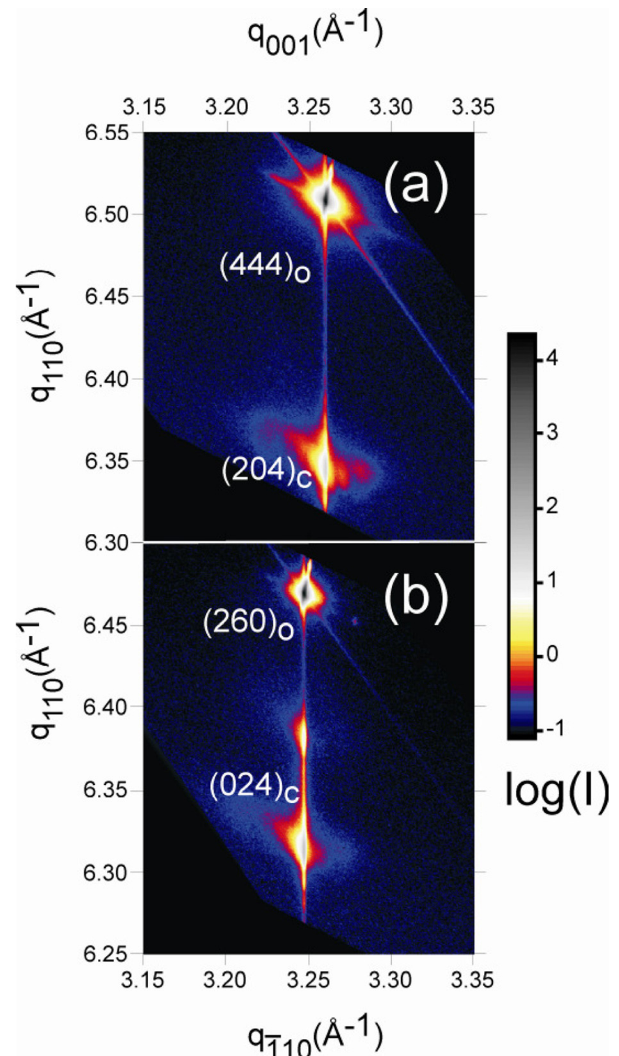

FIG. 7. X-ray reciprocal space maps of a 50 nm $NaNbO_3$ film on a $NdGaO_3(110)_o$ substrate in the vicinity of the $(444)_o$ (a) and $(260)_o$ (b) Bragg reflections.

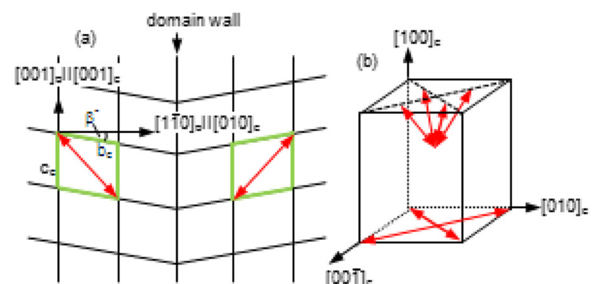

FIG. 8. (a) Schematic drawing of the monoclinic unit cell of $NaNbO_3$ (green) and the possible polarization vectors (red) from bird view (a). In (b) the alignment of the polarization vectors in fully strained films on the $ReScO_3$ substrates only with an in-plane component (lower double arrows) and in partially relaxed films on a $GdScO_3$ substrate with an in-plane and out-of-plane component (upper double arrows) are shown.

[This article is copyrighted as indicated in the article. Reuse of AIP content is subject to the terms at: http://scitation.aip.org/termsconditions. Downloaded to] IP: 134.94.122.17 On: Wed, 18 Jun 2014 12:54:53

compressively (tensily) strained films on $NdGaO_3$ (on $DyScO_3$, $TbScO_3$, and $GdScO_3$) substrates. This behavior can be explained within the framework of the linear theory of elasticity.[53] However, while the experimentally determined $\Delta V/V$ for the compressively strained films on $NdGaO_3$ can be verified by typical Poisson ratios for perovskites,[54] the observed volume changes $\Delta V/V$ for the films under tensile strain are significantly higher than expected from elasticity theory. This deviation points to a slight oxygen deficiency in these films[55,56] and is attributed to the beneficial effect of the formation of oxygen vacancies in order to reduce the lattice mismatch for films which grow under tensile lattice strain.[57]

Partially relaxed films on $ReScO_3$ with Re = Dy, Tb, Gd

PFM data in Figs. 5(a)–5(c) show that domain formation critically depends on the magnitude of lattice mismatch. Generally, the regular arrangement of the a_1/a_2 multi-domains in films of approximately equal film thickness is increasingly deteriorated with increasing lattice mismatch, i.e., from films on $DyScO_3$ (smallest lattice mismatch), to films on $TbScO_3$ to those on $GdScO_3$ (largest lattice mismatch).

While domains in ~30 nm thick films on $DyScO_3$ are well-ordered and continuous over several μm (Fig. 5(a)), the x-LPFM images of $NaNbO_3$ on $TbScO_3$ already exhibit some domain splitting (an example is marked by the arrow in x-LPFM image in Fig. 5(b)). A more complex pattern is observed for films on $GdScO_3$ (Fig. 5(c)). Here, the LPFM images reveal the occurrence of stripe domains also aligned in $[1\text{–}10]_o$ direction, displaying that 90° variants of the a_1/a_2 multi-domains have additionally been evolved. Corresponding GIXRD results (not shown here) point out that monoclinic domains occur which are distorted both in $[1\text{–}10]_o$ (or $[100]_c$) and $[001]_o$ (or $[001]_c$) direction. Furthermore, the VPFM phase images for films on $GdScO_3$ with $d \approx 30$ nm show high contrast between adjacent regions indicating a domain structure of alternating out-of-plane polarization.

The transition from a pure 1D stripe domain alignment to a 2D domain configuration, as indicated in the LPFM images in Fig. 5(c), is assumed to be caused by lattice relaxation and defect formation. Effect of plastic lattice relaxation, as a consequence of lattice mismatch between film and substrate material, can also be observed when film thickness is increased. This has been described in detail for a series of $NaNbO_3$ thin films with different thickness on $TbScO_3$ substrates in Ref. 24. We assume that the exclusive 1D arrangement of the stripe domains in thin fully strained films is provoked by the anisotropic tilting of the oxygen octahedra in the substrate.[58] Thus, the symmetry of the $ReScO_3(110)_o$ surfaces is not fourfold, but rather twofold according to the positions of the Re and O atoms. When the film lattice starts to relax and does no longer "feel" the asymmetry of the substrate's bulk lattice,[59] we suppose that a 2D arrangement develops since the energy difference for both configurations is supposed to be small. Since the lattice mismatch for $NaNbO_3$ thin films on $GdScO_3$ substrates is larger than for films on $DyScO_3$ and $TbScO_3$ substrates, even for the thinnest film on $GdScO_3$ (~10 nm film thickness) the film lattice is partially relaxed resulting in a 2D domain pattern as revealed from the in-plane piezoresponse signal (Fig. 5(d)). For this film thickness (~10 nm), any out-of-plane piezoresponse vanishes, indicating a 2D a_1/a_2 multi-domain configuration (schematically presented by the four double arrows on the bottom of the unit cell in Fig. 8(b)). However, with increasing film thickness increased formation of defects reduces the incorporated lattice strain and a significant enhancement of the out-of-plane piezoresponse with a resulting clear contrast between adjacent domains can be detected (Fig. 5(c)). Possible polarization vectors are schematically illustrated by the double arrows in the top part of the unit cell in Fig. 8(b) indicating the occurrence of a $(c + a_1/a_2)$ multi-domain state[18,60] or M_B domains.

Strain induced domain transitions

Up to here, we can summarize that the phase transition pathway from high compressive to high tensile lattice strain can be roughly sketched by the following sequence: O $\rightarrow$ M_A $\rightarrow$ $(c + a_1/a_2)$ or M_B $\rightarrow$ a_1/a_2 (path 1 in Fig. 6(b)). Christen *et al.*[46] reported, in parts, a resembling trajectory for compressively strained $BiFeO_3$ films which, however, starts from a tetragonal T phase and pass to the rhombohedral R phase (in the R phase the polarization vector is aligned along the $\langle 111 \rangle_c$) via the monoclinic M_C and M_A phases (path 2 in Fig. 6(b)). Instead of the orthorhombic O phase in our system, they observed a quasi tetragonal T phase which is caused by the equal in-plane dimensions of the $LaAlO_3$ lattice and the rhombohedral symmetry of unstrained $BiFeO_3$. In the M_C phase, the polarization vector is rotated from the $[001]_c$ direction in the tetragonal phase towards $[101]_c$ and P is parallel to $\langle u0v \rangle_c$ as indicated by the arrow M_C in Fig. 6(b). The existence of an intermediate M_C phase where the polar vector is rotated away from the $[101]_c$ direction in the orthorhombic phase towards $[001]_c$ could not be verified by RSMs in our $NaNbO_3$ films.

The phase transition from the orthorhombic O phase to the monoclinic M_A phase and finally to the a_1/a_2 multi-domain phase in Fig. 6(b) provokes a rotation of the polarization vector with initially strong out-of-plane component to an exclusively in-plane arrangement. Thereby, it is obvious that the effective piezoelectric coefficient d^{eff}_{zz} decreases with decreasing average in-plane strain as shown in Fig. 9. Simultaneously, we observed a transition from a ferroelectric relaxor in the M_A phase (and presumably in the O phase) in films under compressive lattice strain to a "normal" ferroelectric behavior in $(c + a_1/a_2)$ or M_B and a_1/a_2 multi-domains in the films under tensile strain. Relaxor behavior in ABO_3 perovskites is typically evoked by compositional or charge disordering,[61,62] but also incorporation of impurities or point defects like oxygen vacancies or related clusters can induce relaxor properties.[63] Oxygen vacancies are expected to occur here rather in the $NaNbO_3$ films under tensile lattice strain. However, no ferroelectric relaxor behavior has been observed in these films at temperatures up to RT, rather C-V measurements have displayed normal ferroelectric properties for films on $DyScO_3$ substrates.[64]

[This article is copyrighted as indicated in the article. Reuse of AIP content is subject to the terms at: http://scitation.aip.org/termsconditions. Downloaded to] IP: 134.94.122.17 On: Wed, 18 Jun 2014 12:54:53

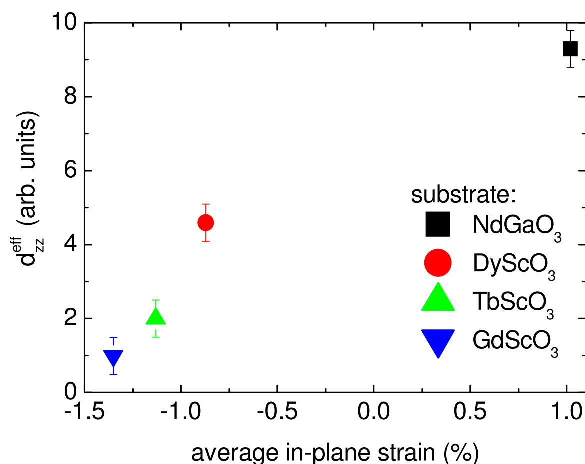

FIG. 9. Effective piezoelectric coefficient d^{eff}_{zz} for 10 nm $NaNbO_3$ films on different substrates as a function of the average in-plane strain.

For the compressively strained films on $NdGaO_3$ substrates, which are assumed to be nearly stoichiometric, we exclude compositional and charge ordering as reasons for the observed relaxor behavior. It is more likely related to substrate induced phase instabilities. The partially relaxed films on $NdGaO_3$ exhibit the low-symmetry monoclinic phase M_A where the polarization vector can freely rotate in the $\{110\}_c$ planes (Fig. 6(a) shows the situation with P in the $(1\text{-}10)_c$ plane) similar to the situation in lead containing perovskites nearby the morphotropic phase boundary like $PbZr_{1-x}Ti_xO_3$ or $PbMg_{1/3}Nb_{2/3}O_{3\text{-}x}PbTiO_3$.[65–67] Furthermore, for the fully strained $NaNbO_3$ films on $NdGaO_3$ with *mm2* symmetry it is known that the *mm2* symmetry can easily be broken by an electric field that is applied in a non-polar direction (e.g., in out-of-plane direction $[001]_c$) which results in a monoclinic M_A or M_C symmetry.[41] In such "rotator" phases the polarization rotation is the dominant mechanism of piezoelectric response. They often offer enhanced piezoelectric properties along non-polar directions and relaxor properties.

Reducing the compressive lattice strain and the transition to tensile lattice strain in the films lead to the occurrence of ferroelectric multi-domain states, as predicted for anisotropic tensile in-plane lattice strain,[17–19] and an enhanced alignment of the polarization vector in the film plane. The crossover to "normal" ferroelectric behavior at RT is tentatively explained by a shift of the transition temperature to higher values as it is known for metal-oxide films under tensile lattice strain.[10,68] In contrast, for compressive lattice strain the transition temperature for $NaNbO_3$ thin films is reduced to about 250 K.[48]

SUMMARY

We have shown that the targeted incorporation of anisotropic lattice strain in $NaNbO_3$ thin films crucially determines the formation of ferroelectric domains. The modification of the strain state of the films from compressive to tensile is accompanied at RT by the transition from weakly ordered domains, which are not resolvable and exhibit large out-of-plane piezoelectric coefficients, to a superposition of two-dimensionally arranged 90° domains. Finally, for commensurate films under high tensile strain a_1/a_2 multi-domains with an elongation of several μm with exclusive in-plane polarization have been found to be well-ordered only in $[001]_o$ direction of the orthorhombic substrates. The symmetry of compressively strained films changes from orthorhombic to monoclinic with decreasing lattice strain, which, in part, resembles the phase sequence nearby the morphotropic phase boundary in lead-containing oxides. Ferroelectric relaxor properties have been attributed to the lowering of symmetry and the related polarization instability. We conclude that due to the application of lattice strain and substrate induced anisotropy the occurrence of low-symmetry phases can be controlled, which provides the unique possibility to grow lead-free oxide films with improved electromechanical properties and anisotropic ferroelectric properties.

ACKNOWLEDGMENTS

The authors would like to thank R. Uecker and his group at IKZ for providing us with high quality rare-earth scandate substrates, A. Devi from Ruhr-University Bochum for the synthesis of suitable precursors, D. Novikov (HASYLAB at DESY), I. Zizak and D. Többens (both BESSY) for assistance in the x-ray experiments, T. Remmele (IKZ) for fruitful discussions as well as S. Markschies and A. Kwasniewski (both IKZ) for technical support.

[1] G. Catalan, J. Seidel, R. Ramesh, and J. F. Scott, Rev. Mod. Phys. **84**, 119 (2012).
[2] A. V. Kimmel, P. M. Weaver, M. G. Cain, and P. V. Sushko, Phys. Rev. Lett. **109**, 117601 (2012).
[3] A. Pramanick, A. D. Prewitt, J. S. Forrester, and J. L. Jones, Crit. Rev. Solid State Mater. Sci. **37**, 243 (2012).
[4] J. S. Speck and W. Pompe, J. Appl. Phys. **76**, 466 (1994).
[5] J. S. Speck, A. Seifert, and W. Pompe, J. Appl. Phys. **76**, 477 (1994).
[6] J. S. Speck, A. C. Daykin, A. Seifert, A. E. Romanov, and W. Pompe, J. Appl. Phys. **78**, 1696 (1995).
[7] J. H. Haeni, P. Irvin, W. Chang, R. Uecker, P. Reiche, Y. L. Li, S. Choudhury, W. Tian, M. E. Hawley, B. Craigo, A. K. Tagantsev, X. Q. Pan, S. K. Streiffer, L. Q. Chen, S. W. Kirchoefer, J. Levy, and D. G. Schlom, Nature **430**, 758 (2004).
[8] D. G. Schlom, L.-Q. Chen, C.-B. Eom, K. M. Rabe, S. K. Streiffer, and J.-M. Triscone, Annu. Rev. Mater. Res. **37**, 589 (2007).
[9] K. J. Choi, M. Biegalski, Y. L. Li, A. Sharan, J. Schubert, R. Uecker, P. Reiche, Y. B. Chen, X. Q. Pan, V. Gopalan, L.-Q. Chen, D. G. Schlom, and C. B. Eom, Science **306**, 1005 (2004).
[10] N. A. Pertsev, A. G. Zembilgotov, and A. K. Tagantsev, Phys. Rev. Lett. **80**, 1988 (1998).
[11] O. Diéguez, K. M. Rabe, and D. Vanderbilt, Phys. Rev. B **72**, 144101 (2005).
[12] Q. Y. Qiu, S. P. Alpay, and V. Nagarajan, J. Appl. Phys. **107**, 114105 (2010).
[13] A. G. Zembilgotov, N. A. Pertsev, U. Böttger, and R. Waser, Appl. Phys. Lett. **86**, 052903 (2005).
[14] C. Zhu and J. Chen, Phys. Lett. A **372**, 81 (2007).
[15] J. Wang and T.-Y. Zhang, Appl. Phys. Lett. **86**, 192905 (2005).
[16] G. Bai and W. Ma, Physica B **405**, 1901 (2010).
[17] G. Sheng, J. X. Zhang, Y. L. Li, S. Choudhury, Q. X. Jia, Z. K. Liu, and L. Q. Chen, Appl. Phys. Lett. **93**, 232904 (2008).
[18] G. Sheng, J. X. Zhang, Y. L. Li, S. Choudhury, Q. X. Jia, Z. K. Liu, and L. Q. Chen, J. Appl. Phys. **104**, 054105 (2008).
[19] Q. Y. Qiu, V. Nagarajan, and S. P. Alpay, Phys. Rev. B **78**, 064117 (2008).
[20] J. Wang, B. Völker, M. Kamlah, and T.-Y. Zhang, Acta Mech. **224**, 1225 (2013).

[This article is copyrighted as indicated in the article. Reuse of AIP content is subject to the terms at: http://scitation.aip.org/termsconditions. Downloaded to] IP: 134.94.122.17 On: Wed, 18 Jun 2014 12:54:53

[21] R. Wördenweber, J. Schubert, T. Ehlig, and E. Hollmann, J. Appl. Phys. **113**, 164103 (2013).
[22] M. D. Biegalski, E. Vlahos, G. Sheng, Y. L. Li, M. Bernhagen, P. Reiche, R. Uecker, S. K. Streiffer, L. Q. Chen, V. Gopalan, D. G. Schlom, and S. Trolier-McKinstry, Phys. Rev. B **79**, 224117 (2009).
[23] K. Kathan-Galipeau, P. P. Wu, Y. L. Li, L. Q. Chen, A. Soukiassian, Y. Zhu, D. A. Muller, X. X. Xi, D. G. Schlom, and D. A. Bonnel, J. Appl. Phys. **112**, 052011 (2012).
[24] A. Duk, M. Schmidbauer, and J. Schwarzkopf, Appl. Phys. Lett. **102**, 091903 (2013).
[25] Y. Saito, H. Takao, T. Tani, T. Nonoyama, K. Takatori, T. Homma, T. Nagaya, and M. Nakamura, Nature **432**, 84 (2004).
[26] Yu. I. Yuzyuk, R. A. Shakhovoy, S. I. Raevskaya, I. P. Raevski, M. El Marssi, M. G. Karkut, and P. Simon, Appl. Phys. Lett. **96**, 222904 (2010).
[27] V. Lingwal and N. S. Panwar, J. Appl. Phys. **94**, 4571 (2003).
[28] S. K. Mishra, N. Choudhury, S. L. Chaplot, P. S. R. Krishna, and R. Mittal, Phys. Rev. B **76**, 024110 (2007).
[29] A. M. Glazer and H. D. Megaw, Acta Crystllaogr., A **29**, 489 (1973).
[30] J. Dec, Cryst. Res. Technol. **18**, 195 (1983).
[31] R. Dirsyte, J. Schwarzkopf, G. Wagner, J. Lienemann, M. Busch, H. Winter, and R. Fornari, Appl. Surf. Sci. **255**, 8685 (2009).
[32] R. Dirsyte, J. Schwarzkopf, G. Wagner, R. Fornari, J. Lienemann, M. Busch, and H. Winter, Surf. Sci. **604**, L55 (2010).
[33] J. Schwarzkopf, M. Schmidbauer, T. Remmele, A. Duk, A. Kwasniewski, S. Bin Anooz, A. Devi, and R. Fornari, J. Appl. Cryst. **45**, 1015 (2012).
[34] M. Schmidbauer, A. Kwasniewski, and J. Schwarzkopf, Acta Crystllaogr., B **68**, 8 (2012).
[35] B. J. Rodriguez, C. Callahan, S. V. Kalinin, and R. Proksch, Nanotechnology **18**, 475504 (2007).
[36] M. C. Morris, H. F. McMurdie, E. H. Evans, B. Paretzkin, H. S. Parker, and N. C. Panagiotopoulos, *Standard X-ray Diffraction Powder Pattern, NBS Monograph 25, Section 18, Data for 58 Substances* (National Bureau of Standards, Gaithersburg, 1981), pp. 64 and 65.
[37] A. Vailionis, H. Boschker, W. Siemons, E. P. Houwman, D. H. A. Blank, G. Rijnders, and G. Koster, Phys. Rev. B **83**, 064101 (2011).
[38] T. Hammerschmidt, P. Kratzer, and M. Scheffler, Phys. Rev. B **75**, 235328 (2007).
[39] I. B. Misirlioglu, S. P. Alpay, F. He, and B. O. Wells, J. Appl. Phys. **99**, 104103 (2006).
[40] A. G. Kalinichev, J. D. Bass, C. S. Zha, P. D. Han, and D. A. Payne, J. Appl. Phys. **74**, 6603 (1993).
[41] M. Davis, M. Budimir, D. Damjanovic, and N. Setter, J. Appl. Phys. **101**, 054112 (2007).
[42] Y. Shiratori, A. Magrez, M. Kato, K. Kasezawa, C. Pithan, and R. Waser, J. Phys. Chem. C **112**, 9610 (2008).
[43] R. Dittmer, W. Jo, J. Rödel, S. Kalinin, and N. Balke, Adv. Funct. Mater. **22**, 4208 (2012).
[44] V. V. Shvartsman, A. L. Kholkin, M. Tyunina, and J. Levoska, Appl. Phys. Lett. **86**, 222907 (2005).
[45] D. Vanderbilt and M. H. Cohen, Phys. Rev. B **63**, 094108 (2001).
[46] H. M. Christen, J. H. Nam, H. S. Kim, A. J. Hatt, and N. A. Spaldin, Phys. Rev. B **83**, 144107 (2011).
[47] Z. Chen, Z. Luo, C. Huang, Y. Qi, P. Yang, L. You, C. Hu, T. Wu, J. Wang, C. Gao, T. Sritharan, and L. Chen, Adv. Funct. Mater. **21**, 133 (2011).
[48] R. Wördenweber, J. Schwarzkopf, E. Hollmann, A. Duk, B. Cai, and M. Schmidbauer, Appl. Phys. Lett. **103**, 132908 (2013).
[49] P. Vousden, Acta Crystllaogr. **4**, 373 (1951).
[50] M. Schmidbauer, J. Sellmann, D. Braun, A. Kwasniewski, A. Duk, and J. Schwarzkopf, "Ferroelectric domain structure of $NaNbO_3$ epitaxial thin films grown on (110) $DyScO_3$ substrates," Phys. Status Solidi RRL (published online).
[51] W. Pompe, X. Gong, Z. Suo, and J. S. Speck, J. Appl. Phys. **74**, 6012 (1993).
[52] A. E. Romanov, W. Pompe, and J. S. Speck, J. Appl. Phys. **79**, 4037 (1996).
[53] J. Sellmann, J. Schwarzkopf, A. Kwasniewski, M. Schmidbauer, D. Braun, and A. Duk, "Strained Ferroelectric $NaNbO_3$ thin films: Impact of PLD Growth Conditions on Structural Properties," Thin Solid Films (submitted).
[54] C. W. Huang, W. Ren, V. C. Nguyen, Z. Chen, J. Wang, T. Sritharan, and L. Chen, Adv. Mater. **24**, 4170 (2012).
[55] C. Wang, B. L. Cheng, S. Y. Wang, H. B. Lu, Y. L. Zhou, Z. H. Chen, and G. Z. Yang, Thin Solid Films **485**, 82 (2005).
[56] T. Zhao, F. Chen, H. Lu, G. Yang, and Z. Chen, J. Appl. Phys. **87**, 7442 (2000).
[57] S. Estradé, J. M. Rebled, J. Arbiol, F. Peiro, I. C. Infante, G. Herranz, F. Sánchez, J. Fontcuberta, R. Córdoba, B. G. Mendis, and A. L. Bleloch, Appl. Phys. Lett. **95**, 072507 (2009).
[58] A. H. G. Vlooswijk, Ph.D. dissertation (University of Groningen, Netherlands, 2009).
[59] J. M. Rondinelli, S. J. May, and J. W. Freeland, MRS Bull. **37**, 261 (2012).
[60] A. L. Roytburd, S. P. Alpay, and L. A. Bendersky, J. Appl. Phys. **89**, 553 (2001).
[61] L. E. Cross, Ferroelectrics **76**, 241 (1987).
[62] A. A. Bokov and Z.-G. Ye, J. Mater. Sci. **41**, 31 (2006).
[63] C.-H. Lee, V. Skoromets, M. D. Biegalski, S. Lei, R. Haislmaier, M. Bernhagen, R. Uecker, X. Xi, V. Gopalan, X. Martí, S. Kamba, P. Kuzel, and D. G. Schlom, Appl. Phys. Lett. **102**, 082905 (2013).
[64] R. Wördenweber, private communication (2013).
[65] M. Davis, D. Damjanovic, and N. Setter, Phys. Rev. B **73**, 014115 (2006).
[66] B. Noheda, Z. Zhong, D. E. Cox, G. Shirane, S.-E. Park, and P. Rehrig, Phys. Rev. B **65**, 224101 (2002).
[67] B. Noheda, D. E. Cox, G. Shirane, R. Guo, B. Jones, and L. E. Cross, Phys. Rev. B **63**, 014103 (2001).
[68] R. Dirsyte, J. Schwarzkopf, M. Schmidbauer, G. Wagner, K. Irmscher, S. Bin Anooz, and R. Fornari, Thin Solid Films **519**, 6264 (2011).

[This article is copyrighted as indicated in the article. Reuse of AIP content is subject to the terms at: http://scitation.aip.org/termsconditions. Downloaded to] IP: 134.94.122.17 On: Wed, 18 Jun 2014 12:54:53